LAWRENCE
LIVERMORE
NATIONAL
LABORATORY

LLNL-BOOK-408177

Present State of Electron Backscatter Diffraction and Prospective Developments

R. A. Schwarzer, D. P. Field, B. L. Adams, M. Kumar, A. J. Schwartz

October 24, 2008

Electron Backscatter Diffraction in Materials Science, 2nd Edition

Disclaimer

1 Present State of Electron Backscatter Diffraction and Prospective Developments

Robert A. Schwarzer[1], David P. Field[2], Brent L. Adams[3], Mukul Kumar[4], and Adam J. Schwartz[4]

[1]Institute of Physics, Clausthal University of Technology, D-38678 Clausthal-Zellerfeld, Germany

[2]School of Mechanical and Materials Engineering, Washington State University, Pullman, WA 99164-2920 USA

[3]Department of Mechanical Engineering, Brigham Young University, Provo, UT 84602-4201 USA

[4]Lawrence Livermore National Laboratory, Livermore, CA 94550 USA

1.1 Introduction

Electron backscatter diffraction (EBSD), when employed as an additional characterization technique to a scanning electron microscope (SEM), enables individual grain orientations, local texture, point-to-point orientation correlations, and phase identification and distributions to be determined routinely on the surfaces of bulk polycrystals. The application has experienced rapid acceptance in metallurgical, materials, and geophysical laboratories within the past decade (Schwartz et al. 2000) due to the wide availability of SEMs, the ease of sample preparation from the bulk, the high speed of data acquisition, and the access to complementary information about the microstructure on a submicron scale. From the same specimen area, surface structure and morphology of the microstructure are characterized in great detail by the relief and orientation contrast in secondary and backscatter electron images, element distributions are accessed by energy dispersive spectroscopy (EDS), wavelength dispersive spectroscopy (WDS), or cathodoluminescence analysis, and the orientations of single grains and phases can now be determined, as a complement, by EBSD.

The first observation of a diffraction pattern in backscattering mode was reported in 1928 by Nishikawa and Kikuchi in the same volume where transmission electron microscopy (TEM) Kikuchi patterns were discussed (Nishikawa and Kikuchi 1928). The researchers placed a recording film to

capture the pattern in transmission, and then placed a film in front of the specimen so as to obtain an image from backscattered electrons. This technique was discussed in detail by Alam, Blackman, and Pashley in 1954 (Alam et al. 1954) and later investigated by Venables and co-workers (Venables and Harland 1973 and Venables and Bin-Jaya 1977). The early literature dubbed the technique high-angle Kikuchi diffraction and it has been referred to by several additional acronyms in the past two decades. Those that are most notable, other than EBSD, include the more accurate nomenclature of backscatter Kikuchi diffraction (BKD) or backscatter electron Kikuchi diffraction (BEKD). (*Note: Acronyms of EBSP, BKP and BEKP are also common in literature and these refer specifically to the image formed by the diffraction technique – i.e., electron backscatter diffraction* ***pattern***.) The terms "electron backscatter diffraction" and "backscatter Kikuchi diffraction" are often used interchangeably in the literature.

Fully automated EBSD has developed into a mature alternative to X-ray pole figure measurements in quantitative texture analysis without the constraints such as ghost problems, defocusing effects, or inconsistent data as a consequence of specimen tilts through large angles. Moreover, automated EBSD has opened new horizons in quantitative texture analysis due to its outstanding high spatial resolution, the access to orientation correlations and orientation stereology, high speed, and the ability to represent the texture and grain boundary character distribution visually and quantitatively via an orientation map. Because SEMs and commercial EBSD systems are readily available, electron backscatter diffraction is no longer an academic technique reserved to only a few select research laboratories, but rather is well on the way to becoming a tool for process development and quality control. Additionally, the technique enables three-dimensional (3D) volumetric reconstruction of the microstructure from consecutive surface sections that are created by mechanical serial sectioning or focused ion beam (FIB) milling as discussed in chapters by Zaefferer and Wright, Groeber, Rowenhort, and Uchic, and Sintay, Groeber, and Rollett. For the purpose of 3D reconstruction and analysis, however, the speed and ease of handling the EBSD system as well as the possibility to re-examine the results at any time are decisive requirements.

Automated EBSD at present is limited to materials with grain sizes larger than several tens of nanometers in diameter and several square millimeters in area can be characterized. Surface strains must not be excessive, and the specimens must be compatible with general requirements of electron microscopy. In particular, the specimens should be conductive and should not decompose in vacuum or under the electron beam. The surface should be reasonably flat and free from foreign layers.

1.2 Generation and Interpretation of Electron Backscatter Diffraction Patterns

EBSD patterns are generated on a phosphor screen by backscatter diffraction of a *stationary beam* of high-energy electrons from a volume of material of crystal approximately 20 nm deep in the specimen times the projected area of the incident beam. The characteristic feature of a backscatter Kikuchi pattern is the regular arrangement of parallel bright bands on a steep continuous background (Figure 1.1) rather than a regular array of diffraction spots as is generated in the TEM in selected area diffraction from a single crystallite. The intersections of Kikuchi bands form prominent and distinct zone axes.

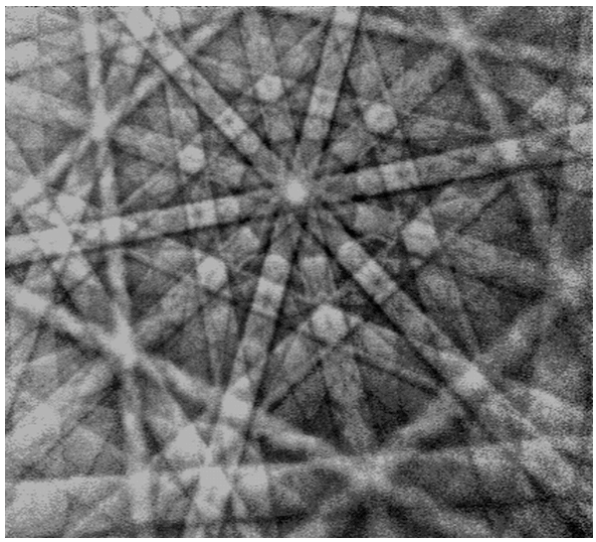

Fig. 1.1 Backscatter Kikuchi pattern from cadmium at 20 keV, acquired with an analog video camera

The geometry of a Kikuchi pattern can be interpreted as a gnomonic projection of the crystal lattice on the flat phosphor screen. The point of impingement of the primary beam on the specimen surface is the center of projection. The lattice planes can be imagined to be stretched out to intersect the screen in the center of the lines of their related Kikuchi bands. Figure 1.2 contains a schematic showing the incident beam on the specimen with a given unit cell orientation and a specified diffracting plane giving rise to backscattered “Kikuchi” diffraction. The two diffracting cones are the edges of the Kikuchi band, and the plane through the center of these cones is the geometric projection of the diffracting plane onto the phosphor screen.

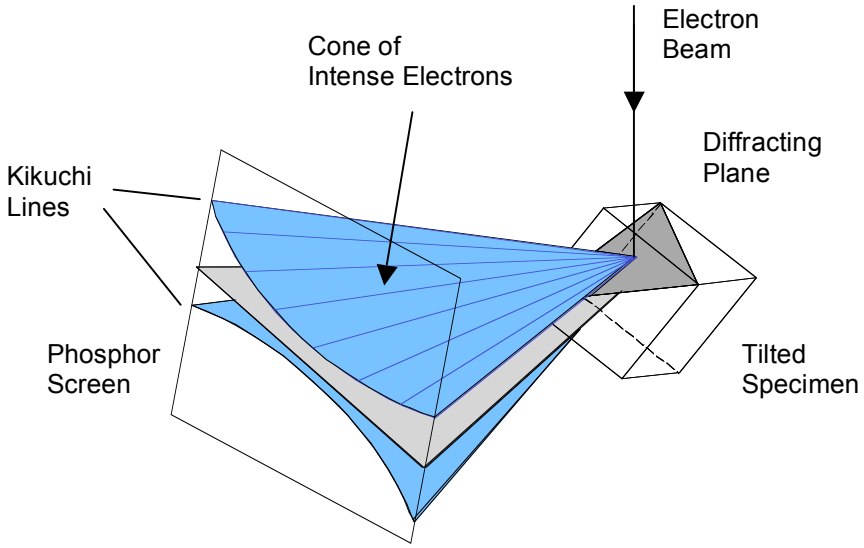

Fig. 1.2 Schematic of the diffracting cones with respect to the reflecting plane, the specimen, and the phosphor screen

When more than one such Kikuchi band is considered, the angles between the projected plane normal orientations correspond to the interplanar angles, and the angular width of a Kikuchi band $\{hkl\}$ is twice the Bragg angle, J_{hkl}. Thus, the width of the bands is related to the interplanar spacing, d_{hkl}, according to Bragg's law,

$$2 \cdot d_{hkl} \cdot \sin \vartheta_{hkl} = n \cdot l \tag{1.1}$$

where n is the order of reflection and l is the wavelength of the incident electron beam, which is dependent on the accelerating voltage of the SEM. The extinction rules for the expected reflections (i.e., Kikuchi bands) of the specific crystal structure are determined by the structure factor of the crystal structure. In addition, higher order reflections may appear as a set of straight lines parallel to the band edges. A decrease in accelerating voltage, U, causes an increase in electron wavelength and hence an increase in the width of the band, which is to a first approximation, $\vartheta_{hkl} \sim 1/U^{1/2}$. An appreciable increase in band width and a deviation from the usual straight-line approximation to the shape of real conical sections is observed at low accelerating voltages in particular for high-order Kikuchi lines.

This simple geometric model and the kinematical approximation do not explain the exact intensity distribution in a Kikuchi pattern. To fully quantify the intensity

distribution, the dynamical theory of electron diffraction must be employed (Reimer 1985). The mechanisms that lead to the formation of the characteristic diffraction contrast features in EBSD patterns, including Kikuchi bands as well as the prominent circular Kikuchi envelopes around zone axes (by appearances like higher order Laue zones (HOLZ) lines from thin foils in convergent beam electron diffraction (CBED)), have been described with the application of dynamic diffraction. Excellent agreement has been obtained between experimental patterns and simulations in extended many-beam dynamical calculations using the Bloch wave approach (Winkelmann et al. 2007; Winkelmann 2008) as is discussed in Chapter 2 by Winkelmann.

1.3 Experimental Set-up of an EBSD System

Instrumentation for generating and capturing electron channeling patterns (ECP) from selected small specimen regions is still available with some commercial SEMs, but the spatial resolution rarely exceeds 50 μm as a consequence of the large spherical aberration of the probe-forming lens and the *pivoting beam*. As a result of the relatively poor resolution and the knowledge that many materials of interest have grain sizes smaller than 50 μm, the EBSD technique has largely taken the place of ECPs in materials and earth sciences investigations. In EBSD, a *stationary beam* is directed onto the grain of interest to form a Kikuchi pattern. The spot size and hence the interaction volume of the primary beam with the crystal contributing to the pattern can be made more than two orders of magnitude smaller than with ECP. Spatial resolution, as well as depth resolution in EBSD, depends on specimen tilt, density of the specimen, and accelerating voltage. The lowest practical beam voltage is about 3 keV if a phosphor screen without an aluminum top layer is used.

For quantitative texture analysis, a statistically significant number of individual grain orientations are required. The interactive, or manual collection of such a database by the operator is both inconvenient and time consuming. Fully automated methods have been developed for acquisition and indexing of Kikuchi patterns within the SEM (Adams et al. 1993) and within the TEM (Zaefferer and Schwarzer 1994; Schwarzer and Sukkau 1998). A number of commercial systems are currently available, which can be added to new or existing SEMs. Automated EBSD systems generally require little operator input; after the initial set up of the system, the only input required is the step size. The EBSD software controls the SEM and rasters the beam across the specimen on a user-specified pre-defined grid, pausing at each point only long enough to acquire the backscatter diffraction pattern, index the orientation, and record the x, y coordinates and the orientation vectors. As discussed in detail below, scanning can be performed either by translating the specimen in *x* and *y* direction with respect to the stationary primary beam with a high-precision computer-controlled specimen stage (Adams et al.

1993), or by stepping the primary beam under digital computer-control across the stationary specimen surface in a similar way as in conventional scanning electron microscopy (Kunze et al. 1994). The positions at which diffraction patterns are measured may constitute some clusters of individual points, a dotted line or a raster field on the specimen surface. For digital beam scanning, a fast and high-resolution (>12 Bit) digital-to-analog (DA) converter is recommended. A fine raster grid allows for very precise positioning of the measured spots on the inclined specimen surface so as to correct for distortions of the grid due to the steep tilt of the specimen surface and the image rotation during dynamical focusing of the probe-forming lens.

1.4 The Components of an Automated EBSD System

An automated EBSD system consists of three main parts that include: the SEM, the pattern acquisition device (or camera), and the software. To achieve the best possible performance, these parts must be considered simultaneously when designing and setting up a system. In general, it is not recommended to construct your own system from scratch. Significant effort is necessary to ensure the coupled system works synchronously and to develop the complex software for controlling the SEM functions, the pattern acquisition, and data interpretation.

The following intrinsic difficulties of EBSD must be addressed:

- steep specimen tilt, approximately 70° relative to the incident beam (see Figure 1.3)
- low contrast and intensity, and high background noise in the backscatter Kikuchi patterns
- disposition to pattern degradation by contamination and deformation layers
- decomposition and charging of low-conducting materials under the beam
- requirements of high speed, high spatial resolution, and high accuracy of measurement.

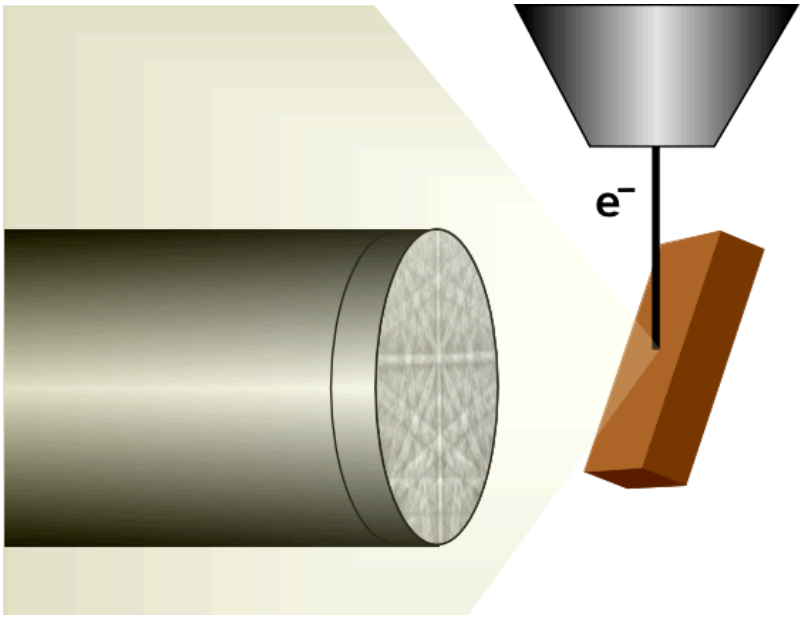

Fig. 1.3 Schematic of the typical EBSD geometry showing the pole piece of the SEM, the electron beam, the tilted specimen, and the phosphor screen

1.4.1 The Pattern Acquisition Device

The backscatter Kikuchi pattern is commonly projected on a transparent phosphor screen (approximately 5 cm in diameter), which is about 2 cm away from the specimen. The screen preferably stands parallel with the primary beam and the tilt axis of the stage, but can be rotated about 20 degrees from that plane in any direction. The pattern is either viewed with a high-sensitivity camera through a window from outside the specimen chamber, or the phosphor screen is placed on a fiber optic bundle, which is directly coupled to the camera sensor. The phosphor screen is generally matched to the spectral response of the sensor for optimum performance. Common phosphors employed for EBSD applications include P20 and P43. P20 has a short decay time at high current densities, which occurs in photon counting tubes, but exhibits a long decay at low current densities. This

latter property is a good match for direct view low light systems. It is yellow/green emitting at 540 nm and has a decay time of about 1-10 ms with an efficiency (lumens/watt) of 30. P43 phosphor is preferred for most applications with TV camera output, because of its efficiency and linearity. It is also fast enough for most high frame-rate applications. It is green emitting (548 nm) with a 1.2 ms decay time and an efficiency of 50. A thin, reflective, aluminum coating is often deposited onto the phosphor screen. This coating enhances the brightness of the phosphor by reflecting light back toward the camera. It also acts as somewhat of a passive energy filter in that it absorbs low energy electrons before they arrive at the phosphor screen. The most important function of the coating is to ground the phosphor screen, as an electrically floating phosphor will charge and degrade the performance of the SEM and will interfere with orientation mapping by automated EBSD. (Alternatively, an indium tin oxide (ITO) layer, or some other conductive and transparent coating, can be deposited on the phosphor screen.)

In most EBSD systems, the acquisition device is mounted on a retractable stage. This enables a precise translation of screen and camera at a fixed spacing from each other along the optic axis of the camera system so that the diffraction pattern projected onto the screen is kept in focus. A travel of several centimeters is required to provide adequate space for bulky specimens when grain orientations need to be measured to the edge of the material. The accurate displacement of the acquisition device can also be used for calibrating the EBSD system with the “pattern magnification method” or “moving screen method” (Day 1993, Hjelen et al. 1993). When retracting the screen from the specimen, the pattern "zooms" out from the pattern center, which can thus be located quite easily. This feature is used to provide an accurate calibration of the system. The pattern center and the specimen-to-screen distance can be accurately calibrated by measuring the locations of several corresponding zone axes on the non-displaced and the displaced patterns. No initial estimates of the calibration parameters and no knowledge of the crystallography of the sample are required. The displacement should be more or less double the initial specimen-to-screen distance for the reference measurement. However, pattern intensity falls off with the square of the specimen-to-screen distance. Furthermore, the precise movement of the device must be done *in situ* under vacuum. In order to guarantee a clean vacuum, a bellows system is recommended over the method of greased O-rings.

There are several types of camera systems that have been used for EBSD image detection. Historically, Peltier-cooled and intensified charge coupled device (CCD) cameras and silicon intensified target (SIT) cameras were used for automated work, and the more expensive slow scan CCD cameras were applied for high quality imaging and phase identification. Currently, CCD cameras are used for both rapid scan rate imaging and for high quality EBSD image collection. CCD cameras can produce binned images on the order of ~100x100 pixels at the rate of near 1000 frames per second with sufficient intensity for reliable indexing. The practical indexing limit is currently in the range of 600 to 800 images per second, but that number is likely to continue to increase with more powerful

computers and optimized image-handling algorithms. To obtain high quality EBSD patterns for phase identification or publication purposes, there is typically no on-chip binning performed and the full image is collected using time averaging techniques to obtain sufficient light intensity and contrast.

Some emphasis has to be placed on the light optics. A high-quality macro lens with a small *f*-stop (large aperture, "fast lens") is a good choice to allow for a short distance between the phosphor screen and the camera sensor chip. Sensitivity of the acquisition system can be almost doubled, at the expense of high cost and practical inconvenience, by coupling the CCD sensor with a (tapered) fiber optic bundle to the phosphor screen. The highest efficiency is expected from on-chip deposition of the phosphor or from direct exposure of the sensor chip to the pattern-forming electrons. Such a sensor chip will presumably be placed inside the specimen chamber, either on a small retractable rod or directly on the specimen stage.

The digital image is the only source of information for pattern recognition. Software can correct for poor image quality or distortions only to some extent. Hence the camera has to be chosen with care, making a trade-off between sensitivity, noise, number of pixels, image quality, and cost. Almost all current EBSD systems have moved to video or digital cameras with solid-state sensors, either to intensified or to integrating CCD cameras. These cameras are economic and the sensor geometry is fixed without producing undue distortions nor "blooming" or burn-in of bright spots (Schwarzer 1989) as has been the case with former vacuum tube sensors. It is worth mentioning that Peltier-cooling of the sensor chip or the photocathode of the image intensifier, in order to reduce noise, is ineffective at short exposures of less than a second.

1.4.2 Mechanical Stage and Digital Beam Scanning

Two computer-controlled sampling modes are used for automated EBSD: stage-scan mode, in which the specimen is translated mechanically under the focused stationary primary beam (Adams et al. 1993), and digital beam scan mode, in which the focused primary beam is moved across the stationary specimen surface (Kunze et al. 1994). The combination of both modes enables large area scans with high accuracy and speed whereby small, slightly overlapping fields are sampled by digital beam scan and stitched together after coarse mechanical steps of the stage from one field to the next.

Advantages of the mechanical stage scan include: the accommodation of large measured fields, only limited in size by the range of travel of the specimen stage; step size calibration does not depend on SEM magnification; there are no geometric distortions resulting from the tilted specimen surface or beam deflection; and from one measured point to the next, diffraction geometry is identical, i.e., pattern center position, specimen-to-screen distance, background

intensity, and focus settings remain constant. Hence, much less elaborate EBSD software is sufficient. A high-performance stage, however, is necessary to keep the specimen surface exactly in the plane of translation. Step sizes less than 0.5 μm in *x* and *y* must be possible. Such a computer-controlled, high precision *x*-*y* stage is a relatively slow and expensive alternative relative to the digital beam scan. In addition, the mechanical stage has a higher uncertainty of the measurement position due to play or lag in the system.

Digital beam scanning, on the other hand, enables an extremely high speed as well as precision in beam positioning. It is cost-effective and not susceptible to breakage. However, the diffraction geometry and pattern center change at each point on the specimen as a result of the varying beam tilt as the beam is stepped across and down the specimen (Figure 1.4). Therefore, the system has to be calibrated dynamically from spot to spot ("*autocalibration*" (Schwarzer 1997)). Otherwise errors in calculated grain orientations may easily exceed several degrees, or indexing of the pattern may fail in particular at low magnifications and with increasing distance of the measured location from that point on which the system had been calibrated initially. Because of the importance of proper calibration, dynamic calibration of the pattern center has been performed on commercial systems since the development of beam scanning in 1994. A simple test on accuracy of calibration can be made by measuring across a large field on a single crystal and checking the uniformity of orientation data. This is also how most systems are calibrated initially. The necessity of a precise calibration of the pattern center as well as the diffraction length (specimen-to-screen distance) has been verified in a computer simulation for transmission Kikuchi patterns by Morawiec (1999).

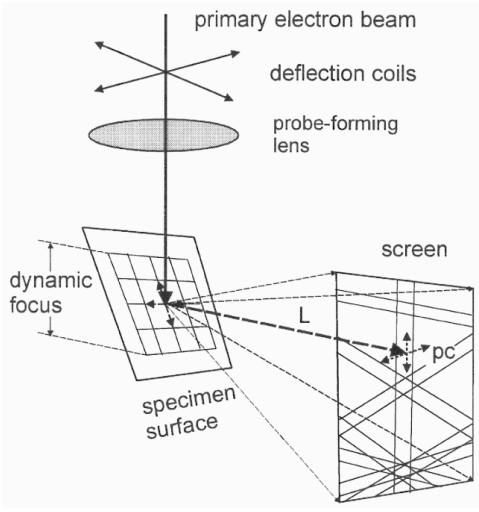

Fig. 1.4 Raster grid on a tilted specimen surface with digital beam scan

The EBSD software must address two additional difficulties with the digital beam scan. As a consequence of the steep forward scattering of electrons, the specimen surface has to be steeply inclined at typically about 20° to the primary beam (i.e. typically 70° from horizontal) in backscatter diffraction in order to generate a Kikuchi pattern of sufficient intensity. When scanning down the specimen line after line, the primary beam spot runs out of focus – increasing in diameter – such that spatial resolution decreases severely. This holds true for low as well as high magnifications because the requirements of high resolution scale with useful magnification. SEM hardware capabilities for dynamic focusing of most SEMs, however, do not accommodate the steep specimen tilts as required for EBSD, nor do they accommodate specimen tilts about an axis at an oblique angle to the axis of the specimen stage. This latter limitation would demand a free port for the camera on that side of the specimen chamber, which is pointing at a right angle on the stage axis.

Defocusing has a detrimental effect on spatial resolution and reliability of indexing, in particular with fine-grain materials, so that dynamic focusing is indispensable not only at low but also at medium magnifications. Pattern quality is a very sensitive indicator of incorrect focus settings due to the diffuseness of Kikuchi patterns. The superposition of two or more diffraction patterns has two adverse effects on indexing. First, the small grains contribute less diffracted intensity to the signal. Their faint patterns are overlooked at best, at the expense of the larger grains, which are covered by the majority of the primary beam spot. Second, spurious bands from faint patterns may be picked up and enter the set of bands for indexing. Pattern interpretation may then fail due to the inconsistency of reflections, or even worse, a false orientation may be the result. The effect of spurious reflections on the reliability of indexing has been clearly demonstrated in a simulation for transmission Kikuchi patterns (Morawiec 1999). The beam aperture is significantly smaller in SEM with a field emission (FE) gun so that the depth of focus is substantially increased and the demand for dynamic focusing on steeply tilted surfaces is alleviated to the same extent.

The steep specimen tilt of about 70° from horizontal causes a further complication of EBSD: the beam spot on the specimen is elongated and hence spatial resolution is reduced in vertical direction by about 3 times. Orientation maps, as well as conventional SEM images, when taken at the same specimen tilt, are foreshortened to the same extent. Therefore, allowance must be made for this kind of image distortion in quantitative stereology either by using different length scales for x and y or by stretching out the foreshortened image.

The signal to noise ratio in EBSD patterns is quite poor. The backscatter Kikuchi pattern is superimposed on a background, which is almost 25 times higher in intensity than the useful signal and depends on the grain orientation, i.e., the actual diffraction pattern. Moreover, the intensity distribution of the background changes during digital beam scans with the position of the beam spot on the

specimen surface as well as with local specimen density (phase) and surface relief. A further fluctuation may be caused by variations of the probe current due to instabilities of the emission current of the gun, drift in the alignment of the column, specimen charging, or build-up of carbon contamination. The quality of diffraction patterns is improved significantly by "flat fielding". In this case, the raw pattern is normalized to a flat field image that contains the background and image artifacts (e.g., scratches on the screen, blind or bright dots on the camera chip), but no features of the Kikuchi pattern. There are several ways to obtain such a flat field image: The beam can be scanned across an area large enough to contain many grains of different orientations. The Kikuchi patterns of these grains are integrated so that they level out to form an even background. The primary beam can also be defocused in spot mode to the extreme so that the Kikuchi patterns fade away. Finally, the background can be reconstructed from the actual diffraction pattern by dedicated software filtering (Field 1997, Schwarzer and Sukkau 1998). In fast EBSD mode (see below) with off-line indexing a sequence of patterns, a flat image can be constructed *a posteriori* by summing up and averaging several patterns out of the sequence that had been acquired at different positions of the beam spot on the sample. Each of these techniques have specific advantages and limitations. Defocused spot mode, for instance, adequately reduces the shadows due to surface relief. Background reconstruction by filtering is particularly useful in case of a coarse grain microstructure or a strong texture.

Consequently, advanced EBSD software has not only to control the digital beam scan or the mechanical stage scan, but in addition has to control the modes of SEM operation (switching between imaging and spot mode) and pattern acquisition (Schwarzer 1997). Switching the SEM between imaging and spot mode is necessary for automated experimental flat fielding. The final lens currents (respectively the working distances and magnification) have to be read for autocalibration and dynamic focusing. The final lens current must be set by the computer as a function of *x*-*y* beam position for software-controlled dynamic focusing. The accelerating voltage is read as a measure of electron wavelength when the band widths are optionally used for indexing.

1.5 Spatial Resolution

A high spatial resolution in orientation measurement is required for the study of fine grain and heavily deformed materials, of recrystallization and grain growth, of grain boundary characterization, and of nanomaterials. But why does the spatial resolution in EBSD fall more than one order of magnitude behind spatial resolution in conventional SEM imaging, and still further behind when compared to the spatial resolution of a TEM? The inherent resolution of EBSD is governed not by the diameter of the beam spot at the point of impact on the surface, but primarily by the excitation volume. That is, the fraction of the interaction volume

of the primary electrons within the sample from where the pattern forming electrons are backdiffracted and leave the crystal without further scattering. The shading in Figure 1.5 indicates this volume fraction. This makes the point of why for orientation microscopy in a SEM it is not wise to reduce the spot size below the diameter of the excitation volume. The adverse effects would be a reduced beam current, hence less intense patterns, and possibly a strong increase in contamination rate by polymerization of hydrocarbons under the beam.

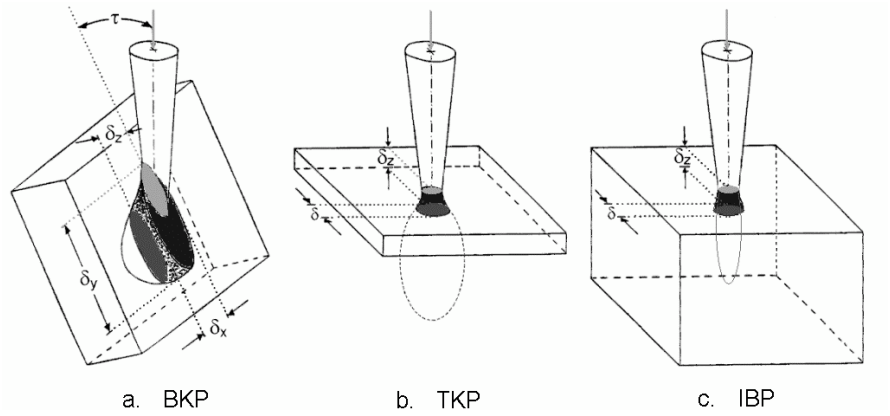

Fig. 1.5 Interaction volume, excitation volume and spatial resolutions, **δ,** with a. Backscatter Kikuchi patterns from a bulk specimen in the SEM, b. Transmission Kikuchi patterns from a thin foil in the TEM, and c. Ion blocking patterns from a bulk specimen in the scanning ion microscope (Schematical representations)

As a consequence of the steep sample tilt, the elongated projection of the beam spot, and the forward scattering, the spatial resolution in EBSD along the beam direction on the sample surface, δ_y, is about three times worse than δ_x. The information depth, δ_z, is limited by the mean free depth of penetration of the backscattered electrons in the sampled material at the actual beam voltage. The excitation volume increases for light materials and high beam voltages. The TEM, on the other hand, is operated at a significantly higher accelerating voltage than the SEM. However, spatial resolution, δ, in microbeam TEM diffraction is still approximately the diameter of the beam size, because the sample is thinned to a thickness in the range of the mean free path of the energetic electrons so that only a small interaction volume can develop (Figure 1.5b). In this case, the information depth, d_z, equals the foil thickness.

Spatial resolution in EBSD can be improved to some extent by lowering the beam voltage from typically 20 kV down to a few kV. However, beam brightness and sensitivity of the phosphor screen, and hence pattern intensity are likewise reduced. While the resolution within a grain is of low significance, it becomes quite critical when the beam approaches a grain boundary. An intelligent pattern

indexing software program can then improve resolution by taking account of the intensity levels of superimposed patterns, rejecting less likely orientation solutions and comparing orientations in neighboring pixels.

Spatial resolution with copper is better than 0.05 μm at 20 kV using a tungsten filament and presently less than about 0.02 μm with a FE gun as a result of the higher beam current in the small probe. This is roughly the same resolution as that predicted by Venables and Harland in 1973. Backscatter diffraction patterns have been found to disappear when a thin foreign surface layer of about twice the thickness of the Rutherford elastic mean free path is present at a given beam energy, i.e., a depth resolution is assumed of about 100 nm for Al, 20 nm for Ni and 10 nm for Au at 40 kV accelerating voltage and 20° angle of incidence to the surface (Michael and Goehner 1994). Theoretical and experimental values of mean free path relate to amorphous materials, but can be significantly larger and orientation dependent in crystals, as a consequence of the channeling effect. Therefore, real information depths in EBSD are expected to be larger than these estimates.

High spatial resolution requires an intense primary beam spot as well as a small interaction volume of the primary electrons beneath the specimen surface. The latter can be reached only by lowering the accelerating voltage significantly from about 20 kV to less than about 5 kV as is usual in present systems with a thermionic cathode. A high beam current in a small spot at low accelerating voltages is the domain of the field emission SEM. Drawbacks of low accelerating voltages are the susceptibility of the beam to magnetic stray fields (hence a small working distance is mandatory which, however, may conflict with the design of current pattern acquisition systems), the low efficiency of present phosphor screens, and the high susceptibility of pattern quality to preparation artifacts or foreign surface layers.

Because spatial resolution depends on the size of the beam spot rather than on the actual magnification of the SEM, a high spatial resolution can be obtained by correct focus settings, irrespective of low magnification. Hence, a large specimen area may be studied by coupling both a mechanical stage and digital beam scan. The accessible specimen area is only limited by the largest field of view of the SEM at the lowest magnification and largest working distance. By slightly oversampling, i.e., by choosing a density of the scanning grid high enough to characterize each grain only a few times on the average, the global texture of a large area can be measured conveniently by orientation microscopy. The advantages over conventional X-ray pole figure measurement are numerous. The selected specimen area is scanned uniformly and the scanned area can be adjusted to irregular shapes. Inhomogeneities in microstructure and texture remain visible in the orientation maps. Consistent data are obtained, whereas data from X-ray pole-figure measurement may be more or less biased due to large variations of specimen tilt, variations of information depth, and variations of the pole-figure window. The angular instrument resolution is usually higher (about 0.5° with EBSD, whereas X-ray pole figures are measured with typically 3° to 5° angular

step width). The X-ray count rate has to be checked for linearity. The ODF calculation from individual grain orientations does not suffer from ghost artifacts. Because almost the same maximum area can be measured with EBSD with digital beam scan and in X-ray pole figure measurements with an oscillation stage, grain statistics are similar and depend on the ratio of average grain size to measured area. Automated EBSD competes well in speed with X-ray diffraction, but is a more universal instrument due to the additional capabilities of the SEM.

1.6 SEM Specifications for Good EBSD Performance

A high beam current is required in spots from 0.02 μm (or slightly less) to 0.5 μm in diameter (to match the material-specific resolution limits of EBSD) at a medium working distance (to accommodate the attachment of the EBSD system and additional detectors), and at accelerating voltages between about 10 kV to 30 kV. A further essential requirement is long-term stability over several hours of the beam current as well as of the mechanics of the specimen stage. Field emission guns have a brightness of about 3 orders of magnitude higher than thermionic emitters, but the cross-over – as the effective source of electrons – is less than 10 nm in diameter, as compared to 10 μm for a LaB_6 emitter. FE guns are superior to any thermionic gun in producing high beam current in small probes of 0.02 μm and less, whereas single-crystal LaB_6 emitters are superior when the beam spot exceeds about 0.5 μm. SEMs with a field emission source enable high currents of several tens of nA in beam spots of a few nm diameter, whereas current in small beam spots drops dramatically when produced with a thermionic emitter gun. Therefore, FE SEMs are the first choice for high speed and high-resolution orientation microscopy. A detector with low sensitivity can be offset by a high beam current only to some extent. It is worth keeping in mind that contamination rate increases rapidly with current density. Therefore, it is wise to focus the beam only down into a useful spot diameter according to the actual grain size and the physical resolution limit of backscatter Kikuchi diffraction that is in the range of some tens of nm, depending on the material and accelerating voltage. Furthermore, a low beam current is generally desirable for the production of patterns to reduce sample damage and charging of low-conductive materials.

Another invaluable advantage of FE guns is the much smaller beam aperture and hence the larger depth of focus. In the range of spot sizes that are of interest for EBSD, performance much depends on the design of the lens system. FE-SEMs are usually optimized for high resolution at low accelerating voltages and short working distances. Cold FE guns in particular suffer from significant current fluctuations and need a regular reconditioning (flashing) after duty periods of about one hour. They are therefore not so well suited for automated EBSD. Schottky FE guns, on the other hand, can reach an adequate long-term stability of the beam current. The main drawback of a FE SEM, however, is the higher costs.

Beam currents of thermionic guns with a conventional tungsten hairpin filament are by about 4 times lower than currents with a LaB_6 cathode. Tungsten filaments are still standard with medium performance SEM since they are fairly economic, need only a moderate high vacuum in the gun chamber, and are known for their excellent beam current stability. In addition, the lifetime of a tungsten filament may easily exceed 150 hours. When changed on a regular basis and operated with some care, the lifetime is a minor source for interruption of long-term scans. In conclusion, a single-crystal LaB_6 gun is a good economic compromise at present, but the trend goes definitively to Schottky FE guns.

A great challenge of automated EBSD is the study of low-conductive surfaces such as minerals, oxides (as discussed in Chapter 27 by Kim and Szpunar), geological samples (as discussed in Chapter 26 by Prior, Mariani, and Wheeler), hard coatings, integrated circuits with dielectric layers, specimens with non-metallic inclusions, or embedded samples. There are several experimental techniques available which intend to either reduce the resistance of the specimen, to reduce the probe current density, to increase the secondary electron emission coefficient, or to compensate for surface charging (Schwarzer 1994). Charging problems are alleviated to some extent by the steep inclination of the specimen surface to the beam. A conductive coating with carbon – not to say gold or other heavy metals – as in conventional SEM surface imaging, however, is prohibitive since any foreign layer degrades pattern quality, as a consequence of the low information depth in backscatter Kikuchi diffraction. A low-vacuum in the SEM specimen chamber is a convenient means by which to suppress specimen charging as described in Chapter 25 El-Dasher and Torres. If available, a "Variable Pressure" SEM working at a chamber pressure in the 1 mbar (100 Pa) range and a beam voltage of about 20 kV or higher is a good choice when insulating materials are in the scope of investigation.

Excessive scattering of the pattern forming electrons on their path to the phosphor screen is an adverse side effect of low vacuum that results in a diffuse pattern. Hence, the shortest possible specimen-to-screen distance and a high accelerating voltage are mandatory to reduce this unwanted scattering of the pattern-forming electrons when working at a low vacuum in the specimen chamber. With decreasing specimen-to-screen distance, a larger angular section of the Kikuchi pattern is captured. The same translation of the beam spot on the sample with digital beam scan results in the same travel of the pattern center on the screen (cf. Figure 1.4), but angular deviation of the reference direction increases with decreasing specimen-to-screen distance. Hence, dynamic pattern center calibration becomes indispensable for correct orientation measurement the closer the screen is placed to the specimen.

An essential requirement is a clean vacuum in the specimen chamber in order to exclude excessive formation of carbon contamination. A turbo molecular pump backed by a dry roughing pump is therefore recommended while greased vacuum sealings should be avoided. The specimen stage should accommodate large specimens and a eucentric tilt from 0° to about 75° from the horizontal plane. The

x-y translation should be made in the surface plane of the specimen. A free port of at least 5 cm wide is required at normal direction to the tilt axis of the stage about 1 cm beneath the eucentric point, for mounting the camera and the phosphor screen. Finally, a fast SEM computer interface is mandatory for high speed digital beam scans, flat imaging, and dynamic focusing. Unfortunately, most high-performance SEMs today are not optimized for automated EBSD. Therefore, a tradeoff has to be made between the performance of the system, the intended applications, and the available hardware.

1.7 The Radon or Hough Transformation for Band Localization

The geometry of a Kikuchi pattern is unique for a particular crystal structure and crystal lattice orientation. The spacing between a pair of lines, i.e., the band width, corresponds to the Bragg angle, and the center line of the band corresponds to the (imaginary) section line of the set of diffracting lattice planes with the screen. Interplanar angles are obtained from the positions of center lines in the pattern. Hence, it is sufficient for indexing to know the *positions and widths* of some bands in the pattern, as the intersection of bands correspond to zone axes or poles. The grain orientation can then be determined with high precision without having to measure band *intensities* in addition, whilst precise orientation determination from spot patterns in the TEM requires the measurement of spot positions as well as their intensities ("intensity center method"). It is worth mentioning here that the angular distance between crystallographic poles does not depend on the acceleration voltage.

Unlike the computer, the human eye can easily perceive lines, curves, and other regular motifs in diffuse or noisy images. Therefore, the user of an EBSD system can interactively extract band positions from a Kikuchi pattern without complications. The extension to a fully automated EBSD system, however, is not so straightforward. The first step for reliable indexing is to detect bands, and then to select the most suitable ones without the operator's interaction. Even though it seems quite simple to automatically attribute individual points or segments of a line from a general array of points to a specific straight line, this challenging task is still difficult to solve with pattern recognition methods. The problem is further aggravated with backscatter Kikuchi patterns, because diffuse broad bands with non-uniform intensity distributions rather than sharp straight lines must be identified on a high background. Therefore, the usual line filtering, gradient, or contour tracing methods are not well suited. The Radon transform (Radon 1917; Deans 1983) or Hough transform (which is a special case of the more general Radon transform) (Hough 1962) is often superior, if the image is noisy and if the motifs to be recognized are fragmentary, but can be described in a parametric form, such as straight lines, circles or conics. A detailed introduction to the theory

and implementations of the Radon transformation has been given by Peter Toft (Toft 1996).

The polar equation of a straight line is

$$r = x \cdot \cos\theta + y \cdot \sin\theta \tag{1.2}$$

r is the distance of the line from the origin, and θ for the angle between the x axis and the normal from the origin to the line. Let f(x, y) be a 2-dimensional function (for our purposes a gray-tone image). The mathematical definition of the Radon transformation of f(x, y) for projections along straight lines is then given as:

$$R(\rho,\theta) = \int_{-\infty}^{\infty}\int_{-\infty}^{\infty} f(x,y)\cdot\delta(\rho - x\cdot\cos\theta - y\cdot\sin\theta)\,dx\,dy \tag{1.3}$$

The Radon transform R(r,θ) is a 2-dimensional integral transformation with the kernel $\delta(r - x\cdot\cos\theta - y\cdot\sin\theta)$. Here, we only consider a discrete Radon transform, which means the image (i.e., the pattern) is made up by a discrete array (x_r, y_s) of image points (so-called pixels), and the Radon space consists of an array of discrete cells on a Cartesian grid (ρ, θ). The integrals in Eq. 3 are replaced by sums. When stepping through the Radon space from one cell (ρ_i, θ_i) to the next, the intensity values of all points (x_i, y_i) on the corresponding Kikuchi line, i, in the pattern are extracted, accumulated, and then stored in this cell (cf. Figure 1.6). A stripe of uniform intensity is so transformed to a butterfly-shaped peak in Radon space. Lines embedded in the stripe are mapped to cells of constant high intensity, whereas lines intersecting the stripe are mapped to cells of reduced intensity according to their section length. If the line or the stripe is fragmented, the accumulated peak intensity is reduced according to the missing sections, but all co-linear image points are still taken into account correctly. Allowance is made for the decrease in line length with increasing distance from the center of the image frame, as well as for image artifacts by normalizing the Radon transformation on a Radon transformation of a flat image of the same size.

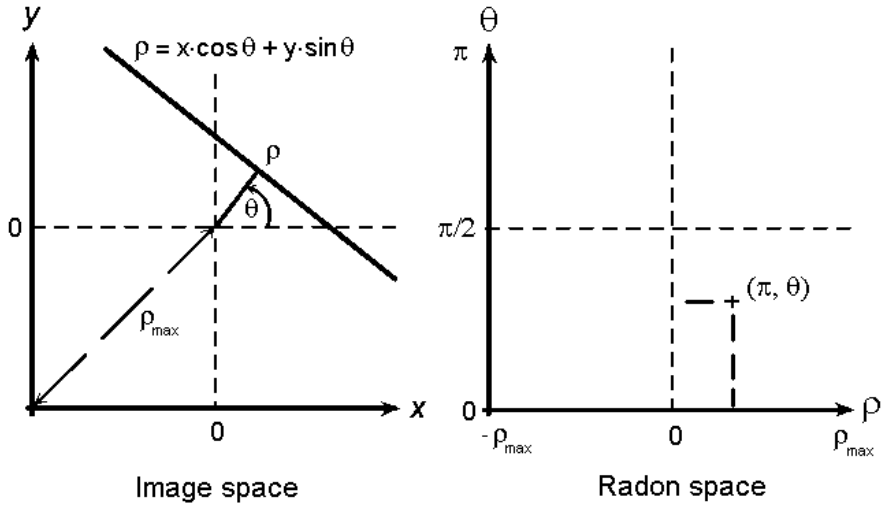

Fig. 1.6 The Radon transformation of a straight line

The task of locating (fragmentary) lines or bands in the diffraction pattern is thus reduced to the simpler task of locating isolated peaks in Radon space. An iteration step can considerably enhance accuracy and save computation time. In a first step, the number of image points in the initial diffraction pattern is reduced by a binning operation before carrying out the transformation. The separation into a high and a low intensity Radon space, R^+ and R^-, reduces interference between dark and bright features in the Kikuchi diffraction patterns, and enables the convenient discrimination of related dark and bright Kikuchi lines (Schwarzer and Sukkau 1998). This separation is recommended in particular for solving transmission Kikuchi patterns and crisp backscatter Kikuchi patterns. The peaks in R^+ space and the cusps in R^- space are then used as "path finders" for one more Radon transformation, but now along stripes in the initial diffraction pattern enclosing the roughly located bands.

The concept of the Hough transform (Hough 1962; Duda and Hart 1972) is similar to the Radon transform. Whereas the Radon transform first accumulates the pixel intensities along a line in the image and then attributes this value to a single cell in Radon space, the Hough transform maps each individual pixel (x_r, y_s) separately from the image onto a sinusoidal curve of constant intensity in Hough space that represents all possible lines through this pixel. Spurious single pixels of high intensity in the image lead to single high-intensity sinusoidal curves. The sinusoidal curves are then overlaid. For co-linear pixels in the image, their sinusoidal curves intersect in a common Hough cell (ρ_l, θ_l) and give rise to a spot whose intensity equals the accumulated intensities along the line in the image. The detection of a line in the image is thus again reduced to the much easier task

of detecting a single spot in Hough space. In case of a Kikuchi band, a "butterfly peak" is finally formed (Krieger Lassen 1994), as is obtained with the Radon transform. So far the results of the Radon and the "modified" Hough transformation of an EBSD pattern are quite similar.

Backmapping can help to concentrate the intensities in Hough space into the most likely peak of the lines of every detected band (Krieger Lassen 1998). A pixel in the image belongs to one line only, unless it is in the rare case the intersection point of lines on crossing Kikuchi bands, and hence should not be mapped into a sinusoid curve, but into a single cell (ρ_l, θ_l) on this curve only. Ideally, this is the intersection point (respectively cell) of all (virtual) sinusoid curves that belong to pixels on the same line in the image. So it is natural to assume that, after overlaying all sinusoid curves of a line, this cell attains highest intensity. A second Hough transformation is therefore calculated, but now the pixels (x_i, y_i) in the image are mapped one after the other by accumulating their intensities only into these cells (ρ_l, θ_l) rather than onto sinusoid curves. The result is a cleaner, more sparse Hough transformation of the pattern. This time-consuming procedure, however, is unnecessary with the Radon transform, since the line intensities are directly projected into the Radon peak of the band whereby the motif can be processed, e.g., by interrogating the lengths of continuous line sections or the intensity profile along the lines.

In present EBSD systems, the automated extraction of band positions from digitized Kikuchi patterns has replaced interactive measurement of band positions by the operator except for system calibration or in case of superimposed patterns.

1.8 Indexing

The so located bands are sorted according to their intensities and widths. Indexing is based on the comparison of measured interplanar angles (which correspond to the angles between the Kikuchi bands) and interplanar spacings (which are represented by the band widths) with theoretical values in a look-up table calculated in advance for the actual crystal structure. Typically, the positions of the 5 to 10 smallest and most intense bands are passed to the indexing routine. Consideration of the first 3 to 4 families of {hkl} planes is usually sufficient for solving a backscatter Kikuchi pattern uniquely in case of high crystal symmetry such as cubic and hcp, whereas increasingly more bands and {hkl} families must be checked and selected in case of pseudosymmetries and lower crystal symmetry. The large angular range of backscatter Kikuchi patterns favors correct indexing. Reference directions in the specimen space (e.g., specimen normal direction and transverse direction in the specimen surface) are finally indexed, and the crystallographic orientation of the grain is described either in (hkl)[uvw] notation, by three Euler angles, (φ_1, Φ, φ_2), or by the rotation matrix, $\mathbf{g}$, which transforms the specimen coordinate system under consideration into the crystal-fixed

coordinate system. A simulated Kikuchi pattern to this solution is finally displayed on the monitor for comparison with the actual diffraction pattern. Detailed algorithms for indexing electron backscatter diffraction patterns have been published by many authors including a complete description in the first edition of Electron Backscatter Diffraction in Materials Science (Schwartz, Kumar and Adams 2000).

The maximum number of indexed bands versus the number of bands that have been considered for indexing a pattern can be used as a measure of probability that a correct solution has been found. There are various ways of defining a statistical "confidence index", "confidence level", or "likelihood" (cf. Field 1997). The quantity is most useful in phase discrimination.

The less perfect the diffracting crystal volume, the more diffuse the corresponding Kikuchi pattern. The blur indicates a high density of point defects or dislocations, lattice strain, thermal lattice vibrations due to the Debye-Waller factor, micro-fragmentation of the lattice, or the superposition of diffraction patterns from several grains sampled at a time by the primary beam spot. A diffuse pattern may also result from a foreign surface layer such as carbon of excessive thickness (which may have been deposited intentionally in order to avoid specimen charging), a contamination layer due to poor vacuum conditions, a deformation layer from inadequate sample preparation, or a defocused electron beam or EBSD detector. The blur can be expressed as a quantity, named "pattern quality", PQ, (or Image Quality, IQ) by measuring the sharpness of some band edges (profile analysis) or the height of peaks in Hough space, or by performing a Fast Fourier Transform (FFT) (Schwarzer and Sukkau 2003) of either the original diffraction pattern or the Radon transformation. Pattern quality maps of coarse grain materials clearly display grain boundaries and surface scratches, and often show features, which appear like a dislocation network. Pattern quality can be used to discriminate between deformed and recovered or recrystallized grains in a microstructure.

1.9 Fast EBSD

A high speed of measurement is not only a value by itself in that the sample throughput of the SEM is improved, but is indispensable for dynamic experiments (e.g., *in situ* tensile and bending test or hot stage experiments as described by Wright and Nowell in Chapter 24 of this volume). For this purpose, a set of individual spot positions, such as in the vicinity of triple points, rather than a regular raster field on the specimen can be selected for consecutive measurements. A short time of measurement will also alleviate some difficulties with long-term stability of the SEM.

Mesh refinement (Schwarzer 1999), also named adaptive orientation imaging microscopy (Yang et al. 1999), is an effective means to increase speed. In a first

step an overview over the microstructure is obtained by scanning on a coarse raster grid with a step size slightly smaller than the diameter of the smallest grains. If intragranular structure is of no concern, it is in principle sufficient to measure the orientation of each grain only once. Therefore, a refined mesh is overlaid of half the step size in the second and of quarter step size in a third loop, but only patterns on those intermediate grid positions will be acquired and evaluated where orientations between neighboring nodal points on the preceding grid differ by more than a preset value. Hence, measurements on the refined meshes in the following passes are concentrated along grain boundaries. Those grid points which could be skipped from measurement are attributed the average orientations of their neighbors. The limitations of this approach are set by small twins that might easily be overlooked in their matrix grains and by a wide distribution of grain size when mesh refinement becomes inefficient since the starting mesh grid has to be rather fine in order to observe the smallest grains.

Geometrical features of interest such as grain boundaries or triple points may also be extracted from SE or BSE images of the microstructure by automated pattern recognition methods and then used to choose the locations for orientation measurement. The prerequisite of this technique named Mesoscale Interface Mapping System (MIMS) (Wu et al. 1999) is a sufficient and unique contrast of the features. Because grains cannot be discriminated with certainty by orientation contrast in a single (BSE) image, a series of orientation contrast images must be acquired either simultaneously with several BSE detectors placed at different angular positions to the specimen, or in sequence with a single BSE detector by varying the specimen tilt to change orientation contrast from one image to the next. If grain boundaries or phases can be recognized due to their relief after a slight etch, the relief contrast in a SE or BSE image can additionally be used to locate these features in the microstructure.

Until 2000, speed of on-line orientation microscopy with an analog camera as the detector was limited by the video frame rate to less than about 30 orientations per second. There was little motivation to further increase the speed of the indexing software. However, after the introduction of digital cameras, the situation has changed. At present, the acquisition speed exceeds 750 patterns per second on suitable samples (Hjelen 2007). Technical details of "*Fast EBSD*" can be found in (Schwarzer 2008a). The essential points of this approach are firstly, the high-speed acquisition and storing of backscatter Kikuchi patterns as a sequence of raw, unprocessed bitmap images, and secondly, the repeatable off-line evaluation of the original pattern sequence.

A high sensitivity of the detector is of key importance for high speed. An enormous advance in image sensor performance has been achieved recently mainly due to the demands of small consumer cameras. Although CMOS sensors are superior in speed, CCD sensors still have a higher quantum efficiency and are more sensitive. Recent electron-multiplying CCD (EMCCD) sensors promise some advantages at very low light levels. A proximity focus image intensifier

between the phosphor screen and the camera can be used to increase overall sensitivity of the detector.

Pixel binning on the sensor chip is a well-proven means to increase sensitivity and speed. (Each individual photo-sensor on the chip array as well as each image point is called a pixel.) The pre-amplifier on the sensor chip is usually optimized for high dynamics and low noise at full pixel resolution and medium to high illumination levels. This is adequate for most situations in machine vision applications. At faint illumination, however, as is the case in backscatter Kikuchi diffraction in the SEM, the working point of the pre-amplifier drops to the flat foot of the current-voltage characteristic curve, hence the signal from one single photo-sensor is submerged by noise. If *n* abutting pixels are bundled together on the chip during the read-out procedure, the current to the pre-amplifier is increased n-fold so as to be raised above the noise floor. Furthermore, the number of pixels per image to be transferred to the computer is also reduced by 1/n, thus speed is likewise increased. Pixel binning ranges from 2 by 2 up to 8 by 8. In principle, a dedicated sensor chip with a coarse array of pixels and correspondingly increased pre-amplification would be superior. Filling factor and capacity per pixel would be higher with the advantage of higher sensitivity and dynamic range. However, the commercial demand for this type of sensors is too small, whereas consumer and machine vision cameras boast of ever increasing pixel numbers.

The camera interface is an integral component of an EBSD system and warrants discussion. Frame grabbers, as common with conventional analog cameras and with machine vision systems in industry using a CameraLink interface, are gradually being replaced by standardized computer interfaces such as USB-2, Firewire and Ethernet. CameraLink has been the interface of choice for professional machine vision applications until lately. It is a fast and rugged solution, which complies with several cameras at the same time. The disadvantages are high costs, clumsy cables, a dedicated frame grabber, and proprietary software.

The main advantages of GigE Vision cameras are low cost, a high bandwidth that enables a very fast transfer of the images from the camera to the computer, and thin and inexpensive cables. A cable length of up to 100 m allows the computer to be installed remotely from the SEM and the data to be transferred through an intranet. The digital signal is, in contrast to analog cameras, little affected by interference with electromagnetic stray fields. A highly welcome feature is the standardization of controlling the main camera functions and data transfer with an easy-to-program protocol. Cameras conforming to the GigE Vision standard protocol GenICam (Generic Interface for Cameras) can simply be exchanged without having to modify the driver or software. This is a particular advantage for EBSD systems, because camera performance makes rapid progress from year to year, indeed faster than personal computers. Hence, with a GigE Vision camera as the backbone of an EBSD detector, a hardware upgrade can conveniently be done from time to time.

At the time of writing this book, the speed of pattern solving with high accuracy approaches 600 to 800 patterns per second. According to web sites as of September 2008, commercial manufacturers of EBSD systems quote indexing rates of 400, at least 400 orientations, and 750 acquired patterns per second on suitable samples. This boost in speed is partially due to improved performance of the computer hardware. The speed of numerical calculations scales with typically 2/3 of the increase in CPU clock rate. Further progress can be made with fast 16 bit DA converters for digital beam control, graphic boards with co-processors, and hard disks. The next generation of solid state hard disks will remove any practical speed limit in storing Kikuchi patterns. The high and uneven background in backscatter Kikuchi patterns can be continually corrected in the camera by subtracting a flat background image pixel by pixel.

A major step ahead has been achieved by improving the software. The speed at which a band can be localized in the pattern scales linearly with the number of pixels in the pattern and the number of (ρ, θ) points in the discrete Radon transformation. The calculation and evaluation of a Radon transformation of 100 by 100 points takes on the average about 10 times longer than indexing the detected bands. Thus, the speed can be quadrupled by simply coarsening the backscatter diffraction patterns and, in conformity, reducing the size of the transformation to one fourth. An unwanted side effect, however, is the much-reduced angular resolution. Depending on pattern quality, a single band can be located in a pattern of 100 by 100 pixels at a typical deviation of $\Delta\alpha = 1.5\text{-}2°$, whereas after coarsening to one fourth of this size the angular uncertainty will be twice as large or worse. Hence, the error limits in the indexing routine have to be widened in order to account for this inaccurate band localization. Even though and as a consequence of this inaccuracy, fewer detected bands are indexed unambiguously. Sometimes this leads to wrong orientations being found and the fraction of points indexed with high confidence may decrease significantly. It is worth mentioning that the grain orientation is calculated as a best fit from the locations of the n consistently indexed bands. Therefore, its mean error is by 1/n less than the mean band deviation. Coarsening the patterns and Radon transformations and, at the same time, allowing a lower reliability of orientation data are appropriate means of increasing speed if only for obtaining a first impression of the texture and of the quality of sample preparation.

The process of separate acquisition and storing of pattern sequences as raw, unprocessed bitmap images is significantly faster than simultaneous acquisition and on-line pattern solving. In addition, off-line pattern solution has many advantages over on-line orientation microscopy, in particular, because pattern interpretation can be repeated at any time by using the original backscatter Kikuchi sequences (Søfferud et al. 2008).

- Dwell time per pattern is constant whereas time for indexing depends on the actual grain orientation and phase.
- No artifacts are induced which frequently occur in on-line indexing when synchronization between the acquisition and interpretation of patterns is lacking.

- The extremely high speed of acquisition is only limited by the sensitivity of the camera and speed of storing the patterns on the hard disk.
- A high acquisition speed is favorable for fast in-situ dynamic experiments.
- A high acquisition speed is economical because the usage time of the SEM is short.
- Cold field emitters with typically low stability are accommodated.
- No compromise is made between speed of acquisition and reliability of indexing.
- Pattern indexing and interpretation can be repeated at any time by using the original diffraction patterns.
- The setting parameters of the indexing program can be optimized conveniently after acquisition.
- Reliability of indexing and the presence of *a priori* unknown phases can be checked.
- Off-line indexing is based on the same philosophy as EDS spectral imaging where complete X-ray spectra are acquired from 2D arrays of points and evaluated off-line.

Due to these advantages, Fast EBSD with off-line solving the acquired pattern sequences will become the standard technique. As an alternative option, acquisition, storage and interpretation of the patterns can be performed on-line as well, but at the disadvantage of reduced speed and reliability.

1.10 Ion Blocking Patterns

Diffraction patterns can be produced not only by electrons or x-rays but also by ions of several tens of keV kinetic energy when impinging on a crystalline surface. They have been recorded on special photographic plates, which cover a large solid angle and are called Ion Blocking Patterns (IBP) (Tulinov 1965). As a consequence of the much shorter deBroglie wavelength and the specific interaction of ions with solid crystals, IBP have, at a first glimpse, an appearance substantially different from the electron backscatter diffraction pattern. Instead of broad Kikuchi bands, the IBPs show narrow straight black bands, almost lines, with a much higher contrast on a flat background (cf. Figure 1.1 and Figure 1.7). However, the geometry of IBP and EBSP is quite similar. Thus, the crystal structure and crystal orientation of the diffracting volume can be determined from the intensity distribution and positions of the bands in an IBP (Barrett 1979) in quite a similar way as in an EBSD pattern.

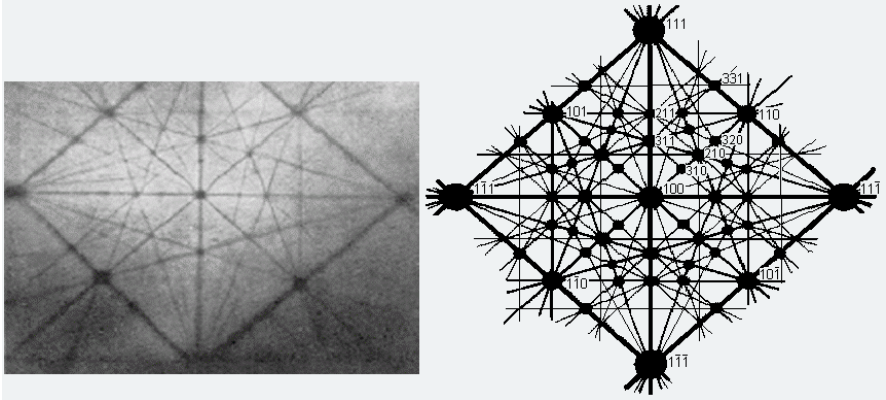

Fig. 1.7 (a) Ion blocking pattern from a (100) face when a 200 keV proton beam impinges on a tungsten single crystal and (b) the simulated pattern (After A.F. Tulinov 1965, Figures 10 and 11). The photographic plate was positioned substantially parallel to the specimen surface.

Intense focused ion beams are produced with liquid metal ion sources or with gas field ionization sources (Tondare 2005). An outstanding high source brightness of more than 10^9 A/cm^{2}sr He^+ ions has been achieved by using a <111> oriented sharp field emitter tip of tungsten so that beam currents up to 100 pA at an energy spread of less than 1 eV and a beam voltage of typically 20 to 30 kV are practical (Morgan et al. 2006). In addition, because both the chromatic and the diffraction aberrations of the probe forming lens are less affected in this set-up, it is expected that it will be possible to focus the beam from the field ionization source into a probe size down to the sub-nanometer range. Thanks to the small excitation volume (cf. Figure 1.5c), a similar high spatial resolution seems possible in ion imaging microscopy and backscatter ion diffraction, which is significantly better than in the SEM.

Ion induced secondary electrons as well as backscattered ions are used for imaging the specimen surface in the scanning ion microscope. An excellent orientation contrast is obtained from polycrystalline surfaces (Wendt and Nolze 2007) (Figure 1.8). This is a clear indication of the strong blocking effect. When the ion beam impinges on the specimen, it is fanned out over large angles due to the onset of inelastic scattering. Further propagation of the ions in the crystal depends on their direction of movement with respect to the lattice. Ions that propagate at angles wider than certain classical critical angles of incidence to densely packed lattice planes or rows of atoms are blocked and backscattered. Up to certain critical angles with respect to the lattice, the ions are channeled deeper in the crystal and experience less probability of being backscattered. Hence, a low signal of backscattered ions as well as secondary electrons is detected at these angles. This classical ballistic model of channeling, based on the assumption of Rutherford scattering, describes the positions of bands in the IBP quite well. The quantum mechanical treatment of ion diffraction must consider a multiple beam

approach (Chadderton 1968). The results correspond to those of the classical treatment, in particular that the band width of IBP is within the mass invariant limit of the critical angle, whereas the width of a Kikuchi band in electron diffraction is given by twice the Bragg angle.

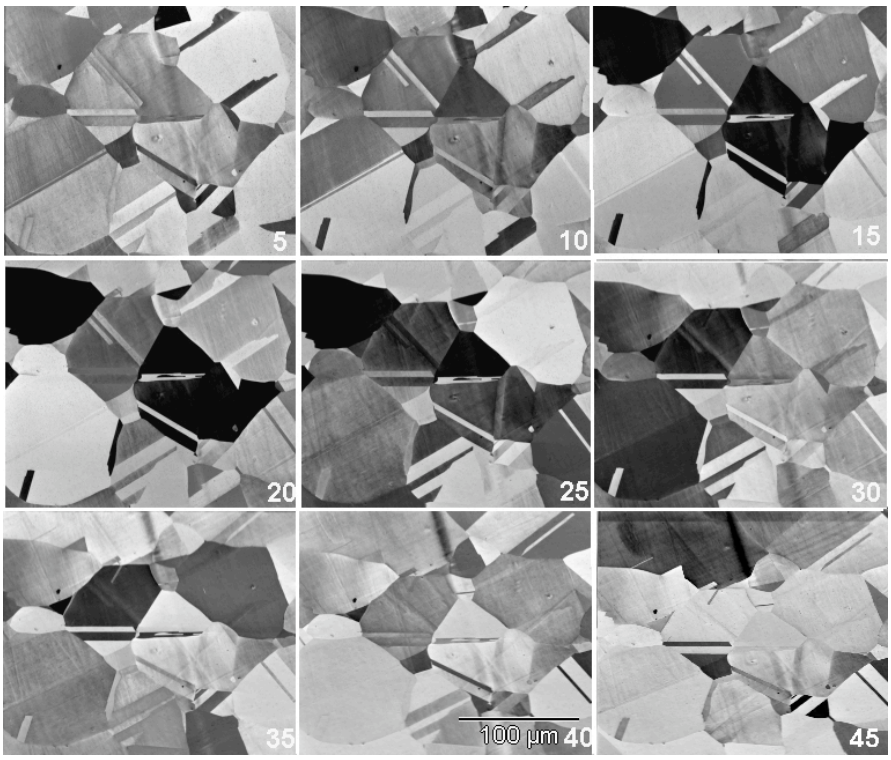

Fig. 1.8 Orientation contrast as a function of specimen tilt in the scanning ion microscope. A polycrystalline copper specimen has been imaged with ion-induced electrons in a scanning ion microscope with a Ga+ liquid metal ion source at 30 keV. The specimen has been tilted about the x-axis of the stage in steps of 5°.

For recording the 2D intensity distribution of the backscattered ions, i.e., the ion blocking pattern, an imaging ion detector is required. Ion-sensitive photographic plates are an impractical recording medium for orientation microscopy. Phosphor screens are a proven means for recording electron diffraction patterns, but they are damaged by ion bombardment such that the sensitivity will drop after exposure to ion blocking patterns. For long-term operation, an open microchannel plate can serve as an ion-to-electron image converter. The converted IBP is projected on a phosphor screen and recorded with a (fiber-optically coupled) CCD camera.

A similar technique as for backscatter Kikuchi diffraction can be used for the acquisition and indexing of IBP. Allowance has to be made in the software for the different background intensities, pattern contrast, and profiles of the Kikuchi bands versus the blocking bands. A schematic set-up of orientation microscopy with IBP and a focused ion beam is shown in Figure 1.9 (Schwarzer 2007, 2008b).

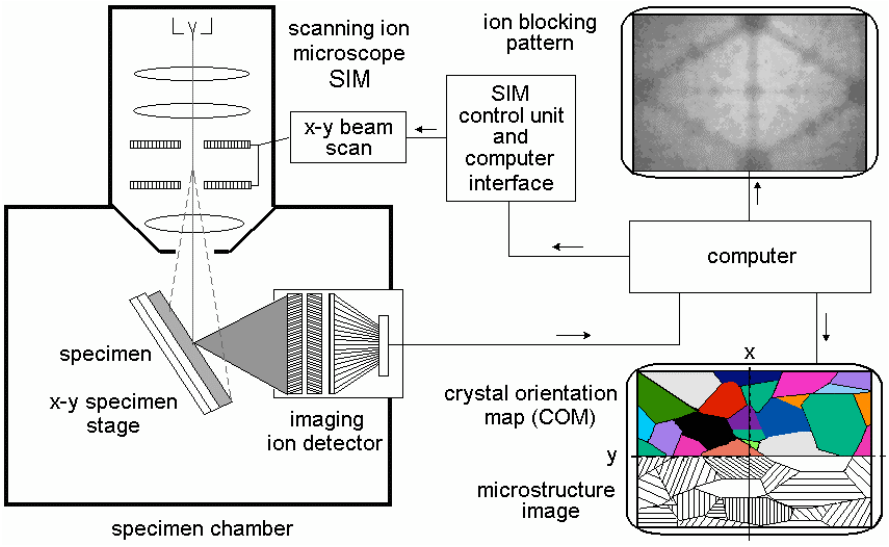

Fig. 1.9 Experimental set-up for orientation microscopy with a computer-controlled scanning ion microscope using ion blocking patterns for grain orientation measurement

The method promises the following advantages over EBSD in the SEM:

- It can be technically realized as an accessory to a scanning ion microscope.
- The sample is tilted at moderate angles of about 45° to the primary beam direction to accommodate the wide-angle pick-up of IBP. As a result, the image distortion and spatial resolution in beam direction are markedly reduced as compared to EBSD where the specimen is steeply tilted to typically 70°.
- Sample preparation is less difficult since deformation layers or foreign surface layers can be removed at a controlled rate *in situ* by using a primary beam of heavy ions until clear blocking patterns have developed.
- 3D reconstruction of the volumetric microstructure from planar 2D slices is facilitated by controlled ion milling. A smooth surface that shows little damage is produced at shallow incidence of the beam. For orientation microscopy the specimen may remain stationary in this position or is simply tilted to a steeper angle to the beam if a higher spatial resolution is required in ion blocking diffraction. In a combined SEM-FIB system, on the contrary, the specimen has to be realigned for grazing incidence FIB surface polishing requiring subsequent delicate tilt-rotation movement of the specimen to return to the EBSD beam position.

- Specimen charging is less harmful than in the SEM because secondary electrons are released from walls of the specimen chamber by the impact of scattered ions and neutrals. They reduce positive surface charging.

Orientation microscopy in a Helium Ion Microscope (Morgan et al. 2006; Scipioni et al. 2007) affords particular advantages:

- A gas field ionization source can be operated with a variety of ionization gases, for example hydrogen, oxygen, nitrogen and noble gases, whereas a liquid metal ion source is limited to produce one species of ions (e.g. Ga^+ or In^+) only.
- When using a primary beam of light ions, as for instance protons or He^+, virtually no specimen sputtering is introduced during orientation measurement nor during imaging. The contamination rate is low.
- The excitation volume is not significantly larger than the minimum spot size. Spatial and in-depth resolution of orientation microscopy with IBP is expected to approach the sub-nanometer range.
- By alternating between a beam of heavy and light ions, a sequential in-depth investigation is performed whereby the specimen is maintained stationary (3D crystal orientation mapping).
- Specimens that adversely react to Ga^+ ions, such as aluminum-based alloys, can be investigated.

1.11 Conclusions

EBSD has become the standard technique for orientation microscopy and texture analysis on bulk polycrystals at a grain specific level. Reasons include the easy operation of commercial EBSD systems, the wide availability of SEM instruments, and high-speed data acquisition. Normal and inverse pole figures, the complete Orientation Distribution Function (ODF) as well as misorientation distribution and orientation correlation functions (ODE, MODE, OCF) can be constructed from the database of individual grain orientations of selected sample areas of any shape. Morphological parameters such as grain size and grain shape distributions as well as crystal lattice related quantities such as crystal perfection and the fraction of recrystallized grains, grain boundaries, misorientations, and the lattice type can be deduced from a set of individual grain orientations.

The study of fine grained and heavily deformed materials, of nanomaterials, of recrystallization, grain growth, and grain boundary characterization often demands a substantially higher spatial resolution than is achieved with EBSD in the SEM. The combination of scanning ion microscopy and ion blocking diffraction promises a high spatial and depth resolution down to the sub-nanometer range in imaging and diffraction mode.

Acknowledgment The ion blocking pattern in Figure 1.7 is a reprint from (Tulinov 1965). The permission for reproduction is gratefully acknowledged to Prof. Dr. A.F. Tulinov, Lomonosov

Moscow State University, and Uspekhi Fizicheskikh Nauk, Moscow. RS would like to thank Prof. Dr. U. Wendt, University of Magdeburg, Germany, for kindly providing the orientation contrast micrograph in Figure 1.8. The work of MK and AJS was performed under the auspices of the U.S. Department of Energy at Lawrence Livermore National Laboratory under Contract DE-AC52-07NA27344.

References

Adams BL, Wright SI, Kunze K (1993) Orientation imaging: The emergence of a new microscopy. Met Trans 24A:819-831

Alam MN, Blackman M, Pashley DW (1954) High-angle Kikuchi Patterns. Proc Roy Soc London A221:224-242

Barrett CS (1979) Ion beam scattering applied to crystallography. Naturwissenschaften 57:287-295

Chadderton LT (1968) A correspondence principle for the channelling of fast charged particles. Phil Mag 8(18):1017-1031

Day A (1993) Developments in the EBSP technique & their application to grain imaging. PhD dissertation, University of Bristol, Bristol, England

Deans SR (1983) The Radon Transform and Some of Its Applications. John Wiley & Sons Inc., New York

Duda RO, Hart PE (1972) Use of the Hough transformation to detect lines and curves in pictures. Comm. ACM 15:11-15

Field D (1997) Recent advances in the application of orientation imaging. Ultramicroscopy 67:1-9

Jarle Hjelen AS, N-7079 Flatåsen, Trondheim, Norway (2007) NORDIF ultra fast EBSD detectors – the UF series http://www.nordif.com

Hjelen J, Ørsund E, Hoel E, Runde P, Furu T, Nes E (1993) EBSP, progress in technique and applications. Textures and Microstructure 20:29-40

Hough PVC (1962) Methods and means for recognizing complex patterns. US patent 3069654

Krieger Lassen NC (1994) Automated Determination of Crystal Orientations from Electron Backscattering Patterns. Ph.D. Thesis, Danmarks Tekniske Universitet, DK-2800 Lyngby

Krieger Lassen N (1998) Automatic high-precision measurements of the location and width of Kikuchi bands in electron backscatter diffraction pattern. Journal of Microscopy 190:375-391

Kunze K, Zaefferer S, Schwarzer R (1994) Orientierungsmapping mit dem Raster-Elektronenmikroskop Beitr. Elektronenmikroskop. Direktabb. Oberfl. 27:169-176

Michael JR, Goehner RP (1994) Advances in backscattered-electron Kikuchi patterns for crystallographic phase identification. In: Bailey GW, Garratt-Reed AJ (eds.): Proc. 52nd Annual Meeting of the Microscopy Society of America San Francisco Press Inc., pp. 596-597

Morawiec A (1999) Reliability of automatic orientation determination from Kikuchi patterns. In: Szpunar JA (ed.): Proc. 12th Intern. Conf. on Textures of Materials NRC Research Press, Ottawa, Vol. 1, pp. 62-67

Morgan J, Notte J, Hill R, Ward B (2006) An introduction to the helium ion microscope. Microscopy Today 14(4):24-31

Nishikawa S, Kikuchi S (1928) The diffraction of cathode rays by calcite. Proc. Imperial Academy (of Japan) 4:475-477

Radon J (1917) Über die Bestimmung von Funktionen durch ihre Integralwerte längs gewisser Mannigfaltigkeiten Ber. Verh. Sächs. Akad. Wiss. Leipzig, Math.-Naturw. Klasse 69:262-267

Reimer L (1985) Scanning Electron Microscopy. Springer Verlag, Berlin, Heidelberg, New York, Tokyo

Schwartz AJ, Kumar M, Adams BL (2000) Electron Backscatter Diffraction in Materials Science. Kluwer Academic/Plenum Publishers, New York. ISBN 0-306-46487-X

Schwarzer R (1989) Die Aufnahme von Reflexions-Kikuchi-Diagrammen im REM mit einer peltiergekühlten, integrierenden CCD-Videokamera Beitr. elektronenmikr. Direktabb. Oberfl. 22:279-282.

Schwarzer RA (1994) Preparation of high-resistance or sensitive samples for grain orientation measurement with electron microscopes. Materials Science Forum 157-162:201-206

Schwarzer RA (1997) Automated crystal lattice orientation mapping using a computer-controlled SEM. Micron 28:249-265

Schwarzer RA, Sukkau J (1998) Automated crystal orientation mapping (ACOM) with a computer-controlled TEM by interpreting transmission Kikuchi patterns. Materials Science Forum 273-275:215-222

Schwarzer RA (1999) Advancements of ACOM and applications to orientation stereology. In: Szpunar JA (ed.), Proc. 12th Intern. Conf. on Textures of Materials NRC Research Press, Ottawa, Vol. 1, pp. 52-61

Schwarzer RA, Sukkau J (2003) Automated evaluation of Kikuchi patterns by means of Radon and Fast Fourier transformation, and verification by an artificial neural network. Adv. Engineering Materials 5:601-606

Schwarzer R (2007) Vorrichtung zur Kristallorientierungsmessung mittels Ionen-Blocking-Pattern und einer fokussierten Ionensonde Patent pending

Schwarzer RA (2008a) A fast ACOM/EBSD system. Archives of Metallurgy and Materials 53:1-6

Schwarzer RA (2008b) Spatial resolution in ACOM – What will come after EBSD. Microscopy Today 16(1):34-37

Scipioni L, Stern L, Notte J (2007) Applications of the Helium Ion Microscope. Microscopy Today 15(6):12-15

Søfferud M, Hjelen J, Karlsen M, Breivik T, Krieger Lassen NC, Schwarzer R (2008), Development of an ultra-fast EBSD detector system. Luysberg M, Tillmann K, Weirich T (Eds.): Proc. 14th European Microscopy Congress EMC2008, Vol.1: Instrumentation and Methods, Springer-Verlag Berlin Heidelberg 2008 ISBN 978-3-540-85154-7, pp.623-624

Toft P (1996) The Radon Transform – Theory and Implementation. PhD Thesis, Danmarks Tekniske Universitet, DK-2800 Lyngby Free download from: http://petertoft.dk/PhD/

Tondare VN (2005) Quest for high brightness, monochromatic noble gas ion sources. J Vac Sci Techn A 23:1498-1508

Tulinov AF (1965) On an effect accompanying nuclear reactions in single crystals and its use in various physical investigations. Soviet Physics - Doklady 10 463-465 (English translation of the original article of A.F. Tulinov in Doklady Akademii Nauk SSSR 162:546-548

Venables JA, Harland CJ (1973) Electron back-scattering patterns—A new technique for obtaining crystallographic information in the scanning electron microscope. Phil Mag 27:1193-1200

Venables JA and Bin-Jaya R (1977) Accurate microcrystallography using electron back-scattering patterns. Phil Mag 35:1317-1328

Wendt U, Nolze G (2007) FIB milling and channeling. G.I.T. Imaging & Microscopy 9(3):34-36

Winkelmann A, Trager-Cowan C, Sweeney F, Day A, Parbrook P (2007) Many-beam dynamical simulation of electron backscatter diffraction patterns. Ultramicroscopy 107:414–421

Winkelmann A (2008) Dynamical simulation of electron backscatter diffraction patterns Chapter 2 This volume

Wu CT, Adams BL, Bauer CL, Casasent D, Morawiec A, Ozdemir S, Talukder A (1999) Mapping the mesoscale interface structure in polycrystalline materials. Microscopy and Microanalysis 5/Suppl. 2:260-261

Yang W, Adams BL, De Graef M (1999) Adaptive orientation imaging microscopy. In: Szpunar JA (ed.), Proc. 12th Intern. Conf. on Textures of Materials NRC Research Press, Ottawa, Vol. 1, pp. 192-197

Zaefferer S, Schwarzer RA (1994) Automated measurement of single grain orientations in the TEM. Z. Metallkunde 85:585-591

Figure captions

Fig. 1.1 Backscatter Kikuchi pattern from cadmium at 20 keV, acquired with an analog video camera

Fig. 1.2 Schematic of the diffracting cones with respect to the reflecting plane, the specimen, and the phosphor screen

Fig. 1.3 Schematic of the typical EBSD geometry showing the pole piece of the SEM, the electron beam, the tilted specimen, and the phosphor screen

Fig. 1.4 Raster grid on a tilted specimen surface with digital beam scan

Fig. 1.5 Interaction volume, excitation volume and spatial resolutions, δ, with a. Backscatter Kikuchi patterns from a bulk specimen in the SEM, b. Transmission Kikuchi patterns from a thin foil in the TEM, and c. Ion blocking patterns from a bulk specimen in the scanning ion microscope (Schematical representations)

Fig. 1.6 The Radon transformation of a straight line

Fig. 1.7 (a) Ion blocking pattern from a (100) face when a 200 keV proton beam impinges on a tungsten single crystal and (b) the simulated pattern (After A.F. Tulinov 1965, Figures 10 and 11). The photographic plate was positioned substantially parallel to the specimen surface.

Fig. 1.8 Orientation contrast as a function of specimen tilt in the scanning ion microscope. A polycrystalline copper specimen has been imaged with ion-induced electrons in a scanning ion microscope with a Ga+ liquid metal ion source at 30 keV. The specimen has been tilted about the x-axis of the stage in steps of 5°.

Fig. 1.9 Experimental set-up for orientation microscopy with a computer-controlled scanning ion microscope using ion blocking patterns for grain orientation measurement